JOURNAL OF PETROLOGY | VOLUME 40 | NUMBER 5 | PAGES 787–806 | 1999

Magmatic Interactions as Recorded in Plagioclase Phenocrysts of Chaos Crags, Lassen Volcanic Center, California

F. J. TEPLEY III[1]*, J. P. DAVIDSON[1] AND M. A. CLYNNE[2]

[1]UNIVERSITY OF CALIFORNIA, LOS ANGELES, DEPARTMENT OF EARTH AND SPACE SCIENCES, LOS ANGELES, CA 90095, USA

[2]UNITED STATES GEOLOGICAL SURVEY, MENLO PARK, CA 94025, USA

RECEIVED APRIL 26, 1998; REVISED TYPESCRIPT ACCEPTED NOVEMBER 17, 1998

The silicic lava domes of Chaos Crags in Lassen Volcanic National Park contain a suite of variably quenched, hybrid basaltic andesite magmatic inclusions. The inclusions represent thorough mixing between rhyodacite and basalt recharge liquids accompanied by some mechanical disaggregation of the inclusions resulting in crystals mixing into the rhyodacite host preserved by quenching on dome emplacement. $^{87}Sr/^{86}Sr$ ratios (~0·7037–0·7038) of the inclusions are distinctly lower than those of the host rhyodacite (~0·704–0·7041), which are used to fingerprint the origin of mineral components and to monitor the mixing and mingling process. Chemical, isotopic, and textural characteristics indicate that the inclusions are hybrid magmas formed from the mixing and undercooling of recharge basaltic magma with rhyodacitic magma. All the host magma phenocrysts (biotite, plagioclase, hornblende and quartz crystals) also occur in the inclusions, where they are rimmed by reaction products. Compositional and strontium isotopic data from cores of unresorbed plagioclase crystals in the host rhyodacite, partially resorbed plagioclase crystals enclosed within basaltic andesite inclusions, and partially resorbed plagioclase crystals in the rhyodacitic host are all similar. Rim $^{87}Sr/^{86}Sr$ ratios of the partially resorbed plagioclase crystals in both inclusions and host are lower and close to those of the whole-rock hybrid basaltic andesite values. This observation indicates that some crystals originally crystallized in the silicic host, were partially resorbed and subsequently overgrown in the hybrid basaltic andesite magma, and then some of these partially resorbed plagioclase crystals were recycled back into the host rhyodacite. Textural evidence, in the form of sieve zones and major dissolution boundaries of the resorbed plagioclase crystals, indicates immersion of crystals into a hotter, more calcic magma. The occurrence of partially resorbed plagioclase together with plagioclase microlites and olivine crystals reflects disaggregation of inclusions and mingling of this material into the silicic host. These processes are commonplace in some orogenic magma systems and may be elucidated by isotopic microsampling and analysis of the plagioclases crystallizing from them.

KEY WORDS: *Chaos Crags; inclusion disaggregation; magma mixing; magmatic inclusions; microsampling*

INTRODUCTION

Magma mixing has been shown to have a large influence on the mineralogical, textural, and geochemical development of arc-related rocks. Undercooled mafic magmatic inclusions in intermediate to felsic rocks provide macroscopic evidence of the exchange between two distinct magmas; resorbed phenocryst phases, compositional and isotopic zoning, and textural discontinuities in the constituent minerals of these lavas record a history of complex mingling and mixing processes (e.g. Singer *et al.*, 1995; Simonetti *et al.*, 1996).

Our research has focused primarily on examining magmatic evolution as recorded in plagioclase phenocrysts. Plagioclase, an almost ubiquitous component in arc-related volcanic rocks, has great potential to provide temporal records of magma chamber dynamics (Anderson, 1983; Stamatelopoulou-Seymour *et al.*, 1990; Blundy & Shimizu, 1991; Singer *et al.*, 1995). It nucleates

*Corresponding author. Telephone: (310) 825-3880. Fax: (310) 825-2779. e-mail: tepley@ess.ucla.edu

at high temperature and persists as a stable crystallizing phase throughout cooling and eruption. Moreover, CaAl–NaSi di usive exchange within the crystal structure is relatively slow, thus ensuring that compositional and textural zoning reflects primary growth (Grove *et al.*, 1984). Chemical and zoning configurations preserved in plagioclase crystals provide information that constrains the changing crystal–melt compositions, and therefore the chemical evolution of the magmas involved.

Compositionally zoned plagioclase phenocrysts are a characteristic and abundant feature of many igneous rocks. Pearce & Kolisnik (1990) have proposed two major types of compositional zoning and have speculated on their petrogenetic origin. Type I zoning is characterized by fine-scale 1–10 μm wide zones, with compositional amplitudes of about 1–10 An %, commonly occurring in periodic, repetitive increments. This type of zonation is thought to reflect near-equilibrium, incremental di usion-controlled growth enhanced by small perturbations within the local reservoir of the growing crystal (Haase *et al.*, 1980; Pearce & Kolisnik, 1990; Pearce, 1993; Singer *et al.*, 1995). Type II zoning, on the other hand, is characterized by zones of thicknesses up to 100 μm, with compositional amplitudes commonly between 10 and 25 An %, and usually associated with a discernible dissolution event (Pearce & Kolisnik, 1990). This type of zoning is controlled by the liquid composition of the system and may reflect gross changes in the crystal's local environment brought on by large-scale disturbance of the crystallizing system such as magma mixing.

Textural and compositional features are common in volcanic plagioclases (Pearce & Kolisnik, 1990; Stimac & Pearce, 1992). Tsuchiyama (1985) has reproduced similar features in the laboratory. In his work, simple dissolution of plagioclase into a melt that is undersaturated with respect to plagioclase may be initiated by a rise in temperature of only a few degrees above the equilibrium liquidus temperature to produce rounded crystals. Additionally, textural and compositional changes in crystals were produced by compositionally disparate interacting liquids and crystals. For example, mantle-like resorbed (sieve-textured) modifications of plagioclase crystals were produced by partial dissolution, a reaction between sodic plagioclase and calcic melt (Tsuchiyama, 1985), the cause of which has been previously attributed to mixing of mafic and silicic magma (Eichelberger, 1978).

Some of the textures and compositional changes described above can also be related to closed-system behavior. Perturbations in the intrinsic variables T, P, X_{H_2O}, reflecting eruptive or convective cycles within a magma chamber, can produce the Type I zoning of plagioclase crystals described by Pearce & Kolisnik (1990). The larger-scale compositional and textural changes are thought to reflect large-scale, open-system processes such as recharge (an introduction of a fresh batch of generally hotter, less evolved magma into the chamber) and/or contamination (assimilation or mixing of a partial melt generated in country rock and its incorporation into the magma). A simple test of open- vs closed-system behavior is to look for isotopic variations within the crystallizing minerals. As minerals crystallize from a magma, they inherit the isotopic composition of the magma from which they grow. The isotopic signatures may be locked into the crystal lattice, or trapped in melt inclusions. If the isotopic composition of the magma changes through magma mixing or assimilation, the changes should be reflected in the progressive growth zones on the crystal. Closed-system processes should not change isotopic values of crystals, parts of crystals, or the rocks in which they reside (with the exception of long-lived systems with very low Sr, high-Rb, high-silica rhyolite; e.g. Bishop Tu , because even in a short amount of time, decay of ^{87}Rb to ^{87}Sr can dramatically a ect the $^{87}Sr/^{86}Sr$ ratio of the system).

At Chaos Crags, in Lassen Volcanic National Park in northern California, emplacement of a series of rhyodacite domes has arrested the mingling of at least two distinct magmas near the initial stages of interaction. In this study, we integrate textural and compositional details preserved in crystals with geochemical and isotopic information to elucidate the processes that produced the erupted lithologies from the Chaos Crags domes. We have focused, in particular, on the isotopic compositions of the key components involved, which serve to fingerprint contributing sources. *In situ* isotopic variations within and between the crystalline phases have allowed us to infer a history best explained by interaction between separate, distinct magmas and their respective crystalline phases involved in an inclusion-forming event or events, followed by mechanical disaggregation of inclusions and concomitant mingling of mineral phases, inclusion fragments, and di erentiated liquids, with the host rhyodacite.

GEOLOGICAL SETTING

Chaos Crags comprise a group of silicic lava domes and associated tephra deposits erupted from the Lassen Volcanic Center, the southernmost extension of current subduction-related magmatic activity of the Cascade Range (Gu anti & Weaver, 1988) (Fig. 1). Volcanism in the Lassen region can be characterized on two scales: (1) regional volcanism comprising hundreds of small (10^{-3}–10^{2} km^3), short-lived, mafic to intermediate volcanoes; (2) focused sustained volcanism involving larger, longer-lived, intermediate to silicic volcanic centers superimposed on the broad platform built by regional volcanism (Clynne, 1990). Included in the focused volcanic centers are a chain of large, late Pliocene to Pleistocene

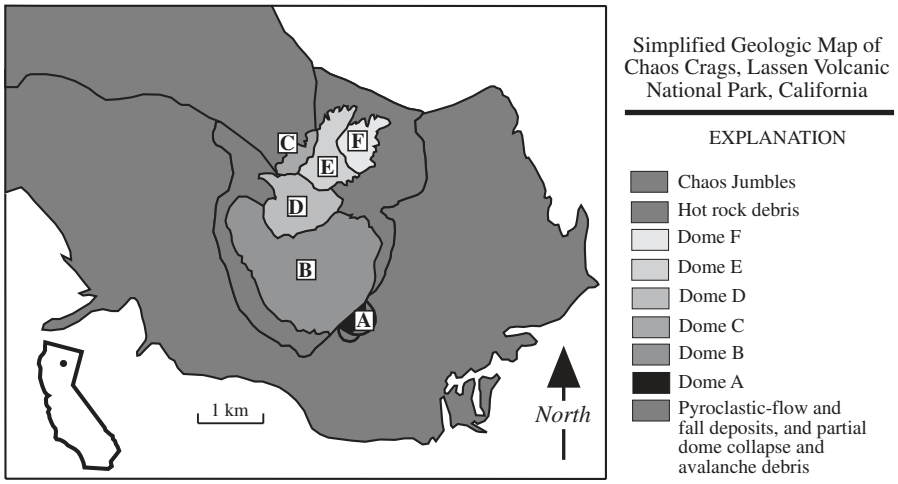

Fig. 1. Simplified geologic map of the Chaos Crags rhyodacite dome complex [modified after Christiansen *et al.* (1999)].

volcanic centers, each of which has flanking silicic domes and flows. Chaos Crags is part of the flanking silicic volcanism of the middle Pleistocene to Holocene, Lassen Volcanic Center (Clynne, 1990).

Detailed geologic mapping (Christiansen *et al.*, 1999) and radiometric dating of carbon samples have established a detailed emplacement history for Chaos Crags, indicating a complex sequence of eruption beginning 1125 years and ending 1060 years (Clynne & Mu er, 1989). The Chaos Crags eruptive sequence was initiated by the formation of a tephra cone and two pyroclastic flows, followed by emplacement of dome A, which plugged the vent. Subsequently, a violent eruption partially destroyed dome A and generated a pyroclastic flow. Emplacement of domes B–F followed, accompanied by hot or warm dome-collapse avalanches from several domes. After a hiatus of ~700 years, Chaos Jumbles formed when dome C produced a series of three cold, rockfall avalanches probably unrelated to volcanic activity (Clynne & Mu er, 1989). The total volume of erupted material approaches 2 km^3.

The lava of the Chaos Crags is porphyritic hornblende–biotite rhyodacite containing 67–70% SiO_2 (the host rocks span the rhyodacite–dacite compositional boundary; rhyodacite will be used to describe all host rocks). The lavas are crystal rich, containing mostly crystals of plagioclase and lesser amounts of hornblende, biotite and quartz. The domes contain a suite of variably quenched, hybrid basaltic andesite to andesite magmatic inclusions composed of sparse olivine, clinopyroxene and calcic plagioclase phenocrysts, and abundant amphibole and plagioclase microphenocrysts (basaltic andesite will be used to describe all inclusion rocks). The inclusions are distributed homogeneously throughout the domes and increase in volumetric abundance and diversity with time throughout the emplacement sequence. Also contained in the host lavas are partially resorbed mineral phases, and small fragments of disaggregated inclusions (phenocrysts and microphenocrysts). This suggests that the inclusions and their fragments were dispersed throughout the domes and have mingled to the extent that crystal populations have exchanged and attained varied degrees of disequilibrium.

There has been some confusion regarding the terminology describing magmatic inclusions, which justifies some introductory definition. In this work we sometimes refer to the hybrid basaltic andesite inclusions as variably quenched inclusions, the textures of which have been best described by Eichelberger (1980). Many of these inclusions have particularly fine-grained to glassy rims and crenulate margins, and all of them contain partially resorbed or reacted phenocrysts from the host lava. These observations indicate that a mixing event between molten host and mafic intruding magma must have occurred before the hybrid inclusion was quenched in or against the cooler host lava. This occurs because the proportion of hotter mafic magma is large compared with cooler felsic magma, allowing the two to hybridize without initially quenching the original basalt liquid in the classic sense (Sparks & Marshall, 1986).

ANALYTICAL PROCEDURES

For bulk chemical analyses, samples were ground in a tungsten carbide shatterbox. Whole-rock major-element compositions were obtained at the US Geological Survey (USGS) laboratory in Denver, Colorado, by wavelength-dispersive X-ray fluorescence (XRF) analysis. Precision of the major-element analyses has been evaluated by repeated analysis of internal standards and was reported by Bacon & Druitt (1988).

Careful petrographic studies of inclusions and rhyodacites were conducted for all Chaos Crags domes, although the current study focuses on early erupted domes, for which the greatest di erence in bulk-rock $^{87}Sr/^{86}Sr$ ratio exists between the inclusions and host. Polished 1–2 mm wafers containing plagioclase crystals in both inclusions and host were prepared.

The Nomarski di erential interference contrast (NDIC) technique (Anderson, 1983; Pearce & Clark, 1989) was used to enhance the compositionally dependent textural features in the plagioclase crystals. Polished probe sections were etched for 180–240 s by immersion in concentrated HBF_4, which preferentially dissolves Ca-rich zones, creating microtopographic ($\pm$0·25 μm) relief. The microtopography is enhanced upon imaging in reflected light. The NDIC technique provides the clearest possible visualization of plagioclase growth structures.

Once imaging of the crystals had been performed, an electron microprobe traverse was taken along a line in the crystal which transects the most growth zones. In this manner, changes in composition (An content) could be related to textural variations. Glasses and mineral phases were analyzed with a Cameca CAMEBAX electron microprobe at UCLA. Element analysis was performed using an accelerating potential of 15 kV, a beam current of 10 nA, and count times of 20 s. We used a defocused beam (~10 μm) for analyzing glasses. Corrections for matrix e ects were made using the procedures of Bence & Albee (1968) with modifications of Albee & Ray (1970).

A low-blank micro-sampling and chemical processing procedure has been set up for isotope analyses of small samples at UCLA. The procedure uses a micro-drill having a vertically mounted bit with an x–y stage. Solid, diamond-tipped drill bits, which range in outside diameter from 0·25 to 0·51 mm, are used to sample the plagioclase crystals at appropriate locations determined through the NDIC and electron microprobe work. A drop of water is placed on the drill site and then, as the drill penetrates, a slurry is created. The slurry is removed by pipette, dried down and weighed, spiked with ^{84}S and dissolved. Sr separation takes place in microcolumns using a stripping technique with Sr-spec® resin or by chromotography with cation-exchange resin, which later proved to be a better method for both Rb separation and maintaining low blanks. After loading on Re filaments with a Ta activator, the sample is analyzed by thermal ionization mass spectrometry.

We have evaluated our ability to analyze $^{87}Sr/^{86}Sr$ ratios accurately and precisely on Sr samples down to 1–5 ng. Both 6 ng and 600 ng NBS 987 standards are routinely analyzed with microsamples, yielding precisions of the order 25 ppm and 15 ppm respectively, with no significant di erence in the measured $^{87}Sr/^{86}Sr$ ratios of the standard (0·710253 $\pm$ 25, n = 9; 0·710234 $\pm$ 15, n = 11, respectively). At lower concentrations, an ion beam of 1–3 V for ^{88}Sr cannot be routinely sustained for a su ciently long period of time to achieve a precision better than ~50 ppm. There is a trade-o between the concentration of Sr in the sample and the weight of material that must be recovered to provide 5 ng of Sr, which in turn is a function of the drill hole size and is deemed a necessary sample size to achieve acceptable precision (see Davidson *et al.*, 1998). Plagioclase crystals, which typically contain >500 ppm Sr, can be sampled with the smallest available drill bits to yield su cient Sr to achieve a precision of ~20 ppm.

PETROLOGY AND GEOCHEMISTRY

A suite of variably quenched, hybrid basaltic andesite inclusions and host rhyodacite was collected from each dome (see Fig. 1). The lavas can be divided into two slightly di erent lithologic groups. Group 1 (dome A, and associated pyroclastic flows, and dome B) are rhyodacitic (SiO_2 > 68%), have fewer and smaller quenched basaltic andesite inclusions, contain a smaller percentage of partially resorbed plagioclase phenocrysts and fragments of disaggregated inclusions, and have biotite and hornblende assemblages that show little or no perceptible opacite-rim development (Fig. 2a). The groundmass is clear colorless glass. Volumetrically, the amount of inclusions in the Group 1 lavas is small (up to 1–2% of total volume). Group 2 lavas (domes C, D, E, F and associated dome collapse deposits and rockfalls) are slightly less evolved (SiO_2 < 68%), have abundant, variably sized, hybrid basaltic andesite inclusions with quenched and unquenched margins, contain abundant partially resorbed plagioclase phenocrysts and fragments of disaggregated inclusions, and, in many cases, have biotite and hornblende crystals with extensive opacite-rim development (Fig. 2b). Although groundmass from Group 2 host lavas is generally devitrified, glassy groundmasses do occur. Group 2 inclusions account for a larger proportion of the total volume of the domes (up to 20%). As the earlier domes (Group 1) are compositionally more evolved than the later domes (Group 2), we suggest (assuming a common source for both) that this reflects progressively greater degrees of mingling or mixing that adds mafic, inclusion-derived components to the host rhyodacite such that it crosses the dacite compositional boundary (~3 wt % SiO_2 di erence).

The hybrid basaltic andesite inclusions consist of a microvesicular network of acicular plagioclase, hornblende, scarce phenocrysts of olivine, clinopyroxene and calcic plagioclase, and abundant (10–20%) interstitial glass (Fig. 2c). The small compositional variation among inclusions can be accounted for by incorporated host-magma liquid and host phenocryst phases enclosed within

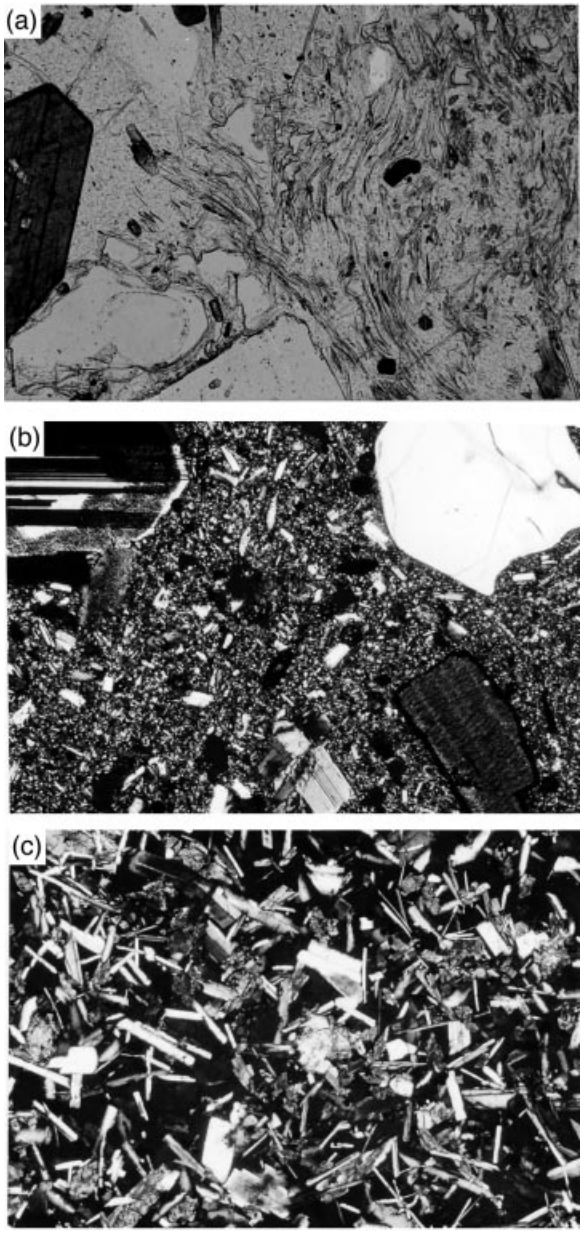

Fig. 2. Photomicrographs showing typical textures of representative dome and inclusion samples. (a) Glass from a Group 1 rhyodacite dome. Field of view is ~2 mm. (b) Devitrified groundmass from a Group 2 rhyodacite dome. Field of view is ~4 mm. (c) Texture of a hybrid basaltic andesite inclusion. Field of view is ~4 mm.

it. The inclusions exhibit a variety of textures from medium-grained aphyric to fine-grained porphyritic (Heiken & Eichelberger, 1980) (Fig. 3). The porphyritic variety contains large (up to 1 cm) plagioclase phenocrysts and other phases thought to have been derived from the host rhyodacite when the inclusion magma intruded. On the whole, the degree of quenching roughly follows the emplacement order (dome A to dome F): inclusions in the early domes are more chilled than those in the later domes. Most inclusions from the earlier domes have a fine-grained matrix with crenulate margins (indicative of a liquid–liquid interface) and little vesiculation (e.g. Bacon, 1986). The later domes have a larger variation in the degree of quenching. Some are quenched hybrid inclusions such as in the earlier domes, but many have fewer quenched textures with varying thicknesses of fine-grained rims and more vesiculation within the inclusions. Many do not have crenulate margins at all because in later domes the inclusions are fragments of once larger inclusions.

Mineral chemistry

The mineral chemistry and textures of major phases in both the inclusions and host reflect the minerals' reaction to exchange between the two di erent magma types or to change in thermal and compositional regime without physical exchange. Compositional descriptions of the mineral phases in host and inclusions were previously provided by Heiken & Eichelberger (1980). Having cursorily and sometimes exhaustively measured compositions of mineral phases by electron microprobe analyses, we include some compositional details of the crystals but focus our discussion on the thermal and compositional e ects of magma mixing. Readers are referred to Clynne (1999) for a detailed description of the textures and compositions of all phases in the 1915 Lassen Peak eruption.

Olivine

Olivine phenocrysts are sparsely present in all lithologies, making up 1% or less of the phenocryst population. Crystals are up to 2 mm in size, and are more abundant in the hybrid basaltic andesite inclusions. In the inclusions, olivine is euhedral to subhedral, smaller ones being less well shaped (Fig. 4a). They have characteristic irregular fracture and are relatively clear. The olivine phenocrysts have little to no reaction with basaltic andesite magma. Representative analyses of olivine reported in Table 1 are similar to compositions reported by Heiken & Eichelberger (1980). The crystals are relatively unzoned from core to rim, having compositions of $Fo_{79–84}$, although Ni concentrations decrease from core to rim.

Olivine crystals also occur in the host rhyodacite, coexisting with quartz phenocrysts (Fig. 4b). These crystals are not as abundant in the host lavas as they are in the inclusions, tend to be smaller, and have reacted with the host rhyodacite, producing either iddingsite or hornblende overgrowths and armoring the crystals from further reaction. However, larger, euhedral olivine crystals surrounded by pyroxene and plagioclase microphenocrysts are also found in the host rhyodacite.

Compositions of olivines in the host are similar to those in the inclusions (Fig. 4c). They are also unzoned and have compositions of approximately $Fo_{79–83}$, with Ni concentrations decreasing from core to rim.

In Fig. 4c, equilibrium liquidus olivine compositions (Fo contents) have been calculated based on $^{Fe/Mg}K_{D\ min/glass}$ values of 0·27–0·33 of Roeder & Emslie (1970). Fo values of olivine crystals produced by rhyodacite compositions range from Fo_{47} to Fo_{52}, and do not match the measured values of $Fo_{79–83}$ (Fig. 4c). However, in the hybrid basaltic andesite inclusions, the equilibrium olivine compositions correspond directly to measured values. Furthermore, Ni concentrations in olivine require K_D values of ~100 for olivine to have crystallized from rhyodacite, which is unreasonable. Our interpretation is that olivines in the hybrid magmatic inclusions and in the host rhyodacite share the same petrogenetic origin and, through inclusion disaggregation, have exchanged from inclusions into the host where they now exist as xenocrysts.

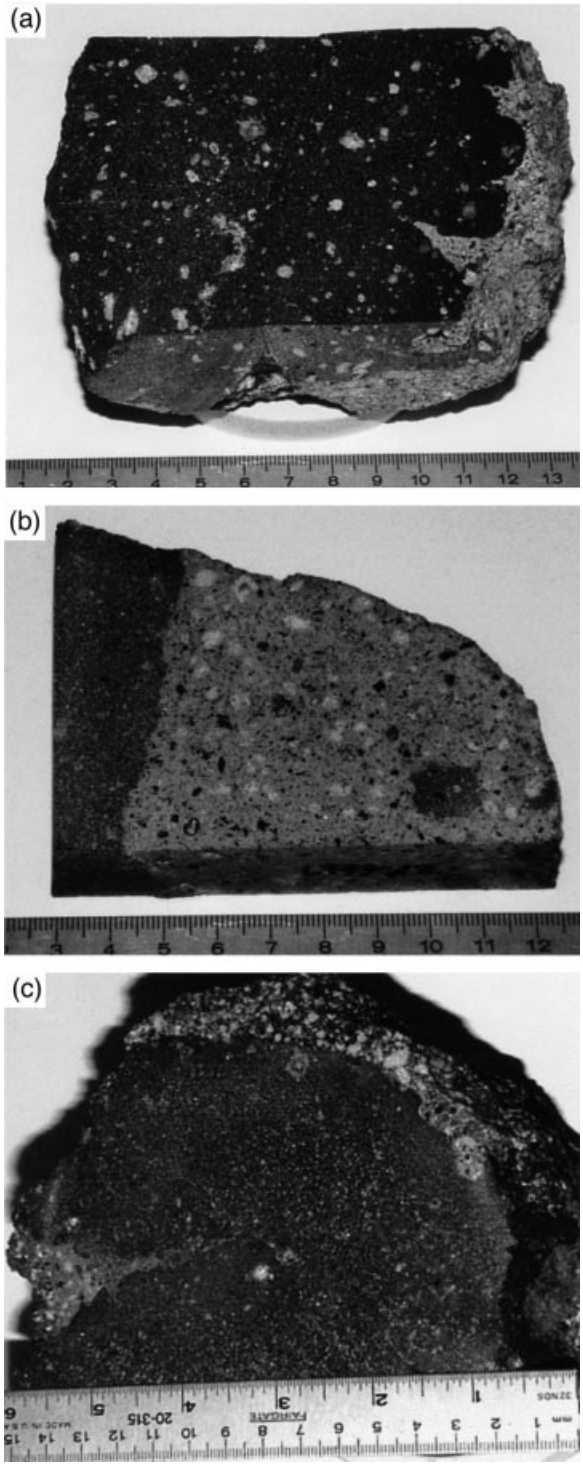

Fig. 3. Sawn and polished slabs of hybrid basaltic andesite inclusions and rhyodacite showing the interface between the two and illustrating the di erent degrees of quenching of inclusions in the Chaos Crags domes. Each field of view is ~15 cm. (a) Hybrid basaltic andesite inclusion and rhyodacite from dome B (Group 1) showing crenulate margin, partially resorbed plagioclase crystals, and fine-grained texture of inclusion. (b) Inclusion and rhyodacite from dome F (Group 2) showing interface between hybrid basaltic andesite inclusion and rhyodacite. The rim of the inclusion is medium grained, probably indicating that this inclusion is a fragment of a larger inclusion that sheared apart in a convecting rhyodacite magma chamber. In this manner, the disaggregating inclusion exposes the interior of the inclusion to the host rhyodacitic magma and allows partially resorbed crystals to be entrained in the host magma. (c) Variably quenched inclusion from dome E (Group 2) showing what appears to be an inclusion folding in on itself, possibly in the act of shearing apart. Part of the inclusion is slightly crenulated with fine-grained margins, and part has medium-grained uncrenulated margins similar to the inclusion above, (b).

Quartz

Quartz phenocrysts are present in all lithologies of the Chaos Crags lavas, accounting for ~1–2% of phenocrysts present. Phenocrysts found in the host rhyodacite are similar from dome to dome; the crystals range in size from 1 to 5 mm, are subhedral to anhedral, rounded, embayed, cracked, and sparsely distributed throughout the lavas (Fig. 5a). Partially resorbed quartz phenocrysts found in the hybrid basaltic andesite inclusions are similar in size and shape to those in the host rhyodacite, although they are slightly smaller, less abundant, and armored by a variably thick rim of clinopyroxene microphenocrysts and dark interstitial glass (Fig. 5b). The clinopyroxene rims probably formed when quartz-bearing rhyodacite mixed with basalt in the inclusion-forming process. A similar process and consequences were described by Clynne (1999) for the Lassen Peak 1915 eruption products, which also involved mixing between silicic and mafic magmas.

Amphibole

Amphibole phenocrysts occur in the host rhyodacite as large, sub- to euhedral phenocrysts, and in the inclusions

Table 1: Representative analyses of olivine in Group 1 (G1) inclusions and in Group 2 (G2) host lavas and inclusions

	G1 inclusion phenocryst		G2 inclusion phenocryst		G2 host xenocryst	
	core	rim	core	rim	core	rim
SiO_2	39·27	39·14	39·32	38·30	39·11	39·34
MgO	42·84	41·53	42·04	41·96	42·60	42·61
FeO	17·48	18·85	19·05	19·49	18·28	18·73
MnO	0·32	0·30	0·31	0·28	0·28	0·22
NiO	0·10	0·07	0·08	0·02	0·12	0·08
CaO	0·12	0·17	0·13	0·16	0·13	0·13
Total	100·14	100·07	100·93	100·21	100·52	101·11
mol % Fo	81·4	79·7	79·7	79·3	80·6	80·2
Ni (ppm)	810	580	620	150	920	660

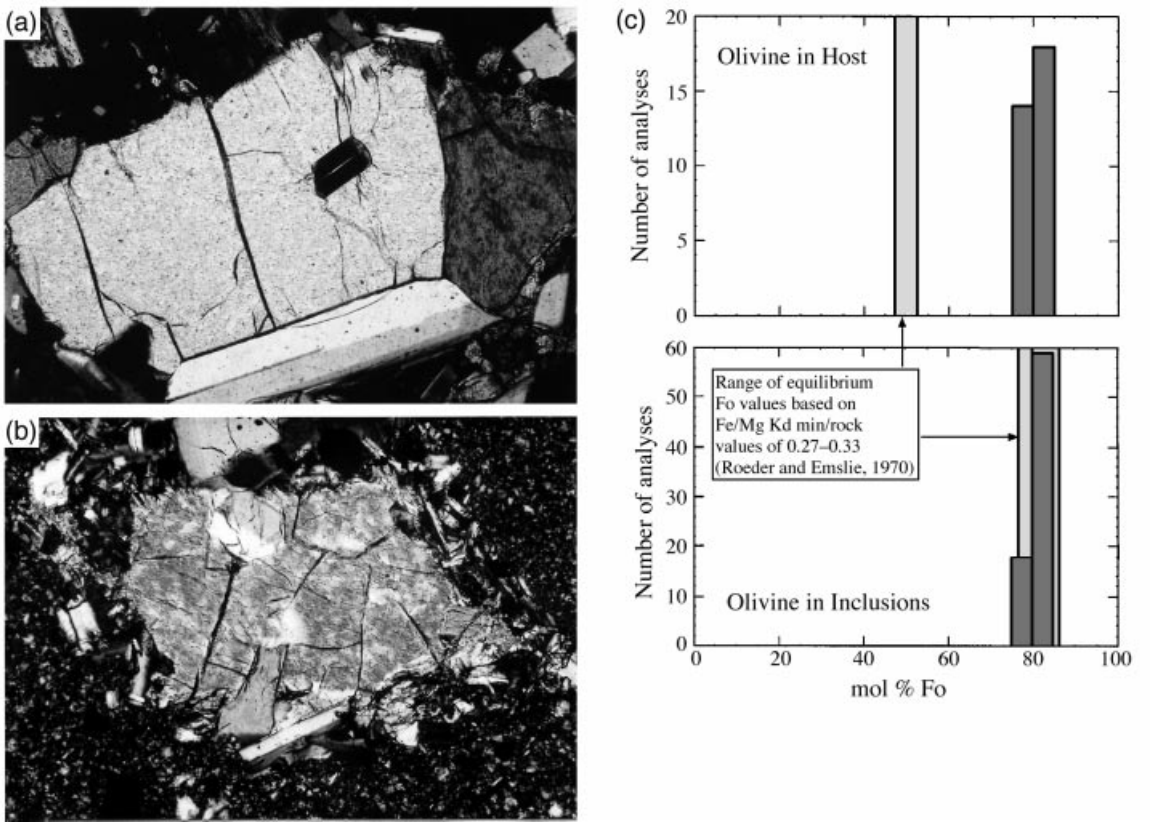

Fig. 4. Textural relations of olivine in the Chaos Crags lavas. Each field of view is ~2 mm. (a) Olivine phenocryst in a basaltic andesite inclusion. The olivine crystal is euhedral to subhedral and shows characteristic irregular fracture. (b) Olivine phenocryst in host rhyodacite lava. The olivine is subhedral to anhedral, and shows increased reaction with host lava. (c) Diagram showing the similarity in compositions (dark-shaded areas) for olivines found in magmatic inclusions and host lavas. Light-shaded areas are equilibrium compositions of olivines calculated from $^{Fe/Mg}K_{D\ min/liq}$ values of 0·27–0·33 (Roeder & Emslie, 1970).

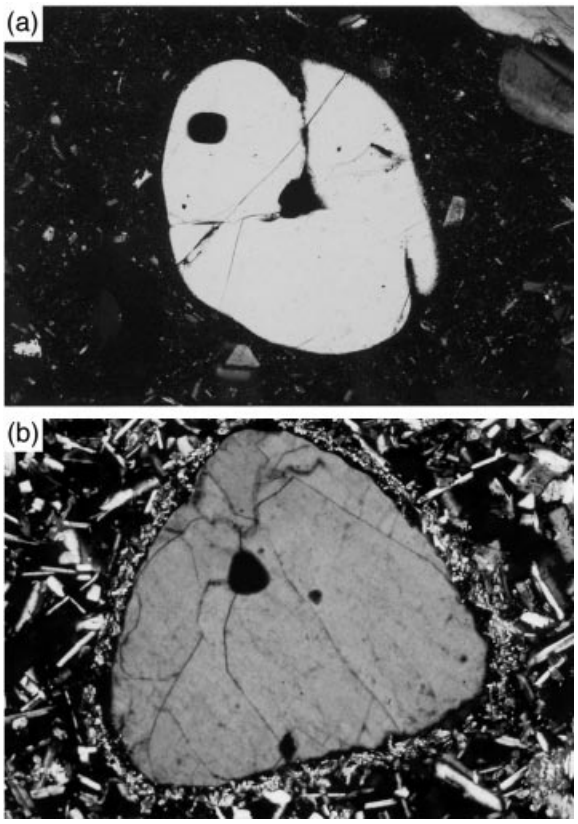

Fig. 5. Textural relations of quartz in Chaos Crags lavas. Each field of view is ~4 mm. (a) Quartz phenocryst in host rhyodacite. The crystal is rounded and embayed but shows no appreciable reaction with surrounding host matrix. (b) Quartz phenocryst in magmatic inclusion. The crystal is partially resorbed and embayed, and shows reaction-rim armoring with clinopyroxene.

as large, partially resorbed phenocrysts and as lath- and diamond-shaped microphenocrysts. In host lavas, amphibole constitutes ~2% of the rhyodacite and ranges in size up to 1·5 mm in basal sections and up to 15 mm in sections parallel to the *c*-axis. Amphiboles in rocks from early eruptions (Group 1) are generally euhedral and display light brown to medium brown pleochroism (Fig. 6a), but those from later eruptions (Group 2) are subhedral, have darker, reddish brown pleochroism, and exhibit a variably thick opacite rim (Fig. 6b). Representative analyses of amphibole from Group 1 and Group 2 lavas are listed in Table 2.

Opacite rims on amphibole are common in arc-related volcanic rocks and need not be related to magma-mixing events. Rutherford & Hill (1993) have demonstrated with the 1980–1986 erupted lavas of Mount St Helens that dehydrogenation of amphibole and the resulting opacite rims may be produced by dehydration of a coexisting melt, owing to a reduction of ambient pressure, as in the case of slowly ascending magmas. Furthermore, they postulated that the ascent rate of the early eruptives,

Table 2: Representative analyses of amphibole phenocrysts in Group (G1) and Group 2 (G2) lavas

	G1 phenocryst		G2 phenocryst	
	core	rim	core	rim
SiO_2	48·29	49·19	49·61	49·56
Al_2O_3	6·89	6·12	5·53	5·75
FeO	13·14	11·92	12·34	11·98
MgO	15·09	15·75	15·53	15·68
MnO	0·58	0·60	0·75	0·55
TiO_2	1·33	1·18	1·00	1·04
CaO	11·32	11·24	11·12	11·19
Na_2O	1·37	1·31	1·13	1·19
K_2O	0·44	0·43	0·36	0·37
Cr_2O_3	0·03	0·01	0·02	0·00
Total	98·48	97·74	97·39	97·31

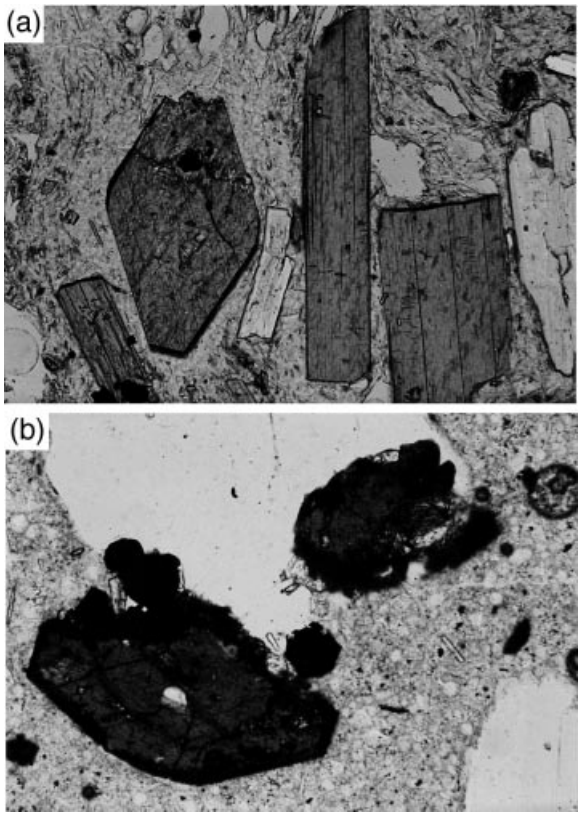

Fig. 6. Textural relations of amphibole in Chaos Crags lavas. Field of view is ~2 mm. (a) Representative amphibole and biotite phenocrysts from Group 1 lava. Euhedral crystals in vitrified glass groundmass should be noted. (b) Representative amphibole phenocrysts from Group 2 lava. The embayed crystal has a moderately developed opacite rim, and resides in devitrified rhyodacitic groundmass.

Table 3: Representative analyses of biotite phenocrysts in Group 1 (G1) and Group 2 (G2) lavas

	G1 phenocryst		G2 phenocryst	
	core	rim	core	rim
SiO_2	37·05	37·49	37·94	37·66
Al_2O_3	13·55	13·63	13·52	13·61
FeO	14·77	14·48	15·18	15·06
MgO	15·02	15·37	15·08	15·13
MnO	0·16	0·24	0·18	0·18
TiO_2	4·25	4·35	4·16	4·09
CaO	0·01	0·00	0·00	0·00
Na_2O	0·50	0·63	0·82	0·81
K_2O	8·74	8·94	8·99	8·86
Cr_2O_3	0·02	0·05	0·04	0·03
Total	94·06	95·18	95·91	95·42

characterized by amphiboles with no reaction rims, is >66 m/h, whereas thick-rimmed amphiboles from later eruptives ascended at about 15–30 m/h. Their explanation is that later eruptives spent up to 25 days along the conduit margins before being mixed into a viscous, slowly ascending dacite. The development of opacite rims on amphiboles of Chaos Crags lavas is probably also the result of dehydrogenation related to slowly ascending magmas, and the interpretation of Rutherford & Hill (1993) for increasingly thick rims may imply a similar eruptive pattern for Chaos Crags. The darker color and pleochroism in amphiboles of Group 2 lavas probably reflects oxidizing conditions during ascent or after eruption.

The inclusions contain two types of amphibole. The most abundant type forms bladed or diamond-shaped microphenocrysts. They are compositionally zoned from cores to rims (e.g. Al_2O_3 varies from ~15 wt % to ~7 wt %; Heiken & Eichelberger, 1980) and can be interpreted as high-temperature primary phases of the inclusions. The other amphiboles in the inclusions are host-derived amphiboles that show varying degrees of recrystallization. This texture represents amphibole converting to aggregates of plagioclase, oxides, and pyroxenes, caused by thermal breakdown.

Biotite

Biotite phenocrysts (Table 3) make up ~1–2% of crystals in the host rhyodacite and occur as partially resorbed crystals in hybrid basaltic andesite inclusions. Biotite phenocrysts range in size from 0·25 mm to 1·5 mm, the larger crystals found predominantly in the Group 1 lavas

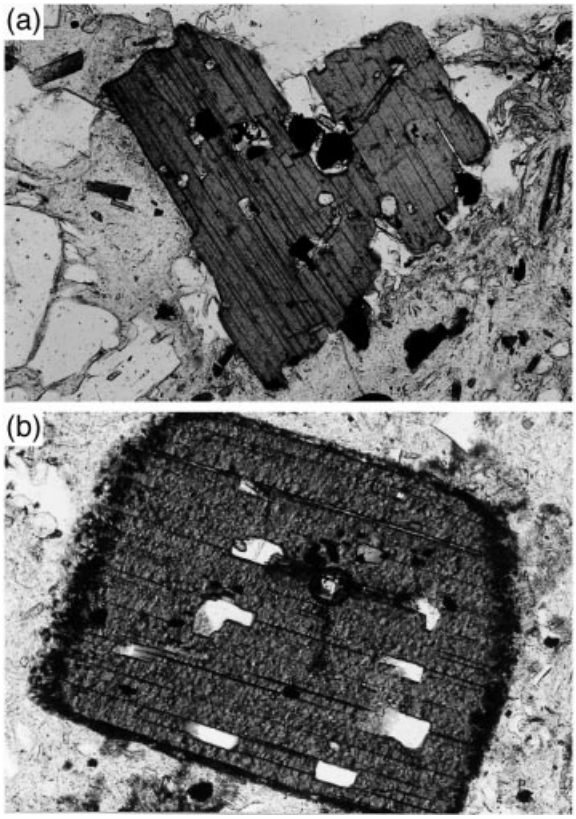

Fig. 7. Textural relations of biotite in Chaos Crags lavas. (a) Representative biotite phenocryst from Group 1 lava. The crystal is euhedral to subhedral, and although speckled with Fe–Ti oxide crystals, shows no development of an opacite rim. Field of view is ~2 mm. (b) Representative biotite phenocrysts from Group 2 lava. This subhedral crystal has a moderately well-developed opacite rim probably owing to decrease in pressure and the resultant dehydrogenation. Field of view is ~2 mm.

(Fig. 7a). Also found in Group 1 lavas are characteristically more euhedral crystals, whereas in Group 2 lavas, crystals tend to be rounded, broken, pitted and sub- to anhedral (Fig. 7b). Crystals have light brown to dark brown pleochroism, although this darkens and becomes reddish brown in Group 2 lavas. Also more predominant in Group 2 lavas are reaction rims around biotite crystals, varying in thickness from tens to hundreds of microns.

Feeley & Sharp (1996) have shown that reaction rims around biotite crystals can be a result of increased heating producing a dehydrogenation reaction in biotite. Opacite rims may also develop, as in amphibole, owing to a decrease in pressure and separation of an aqueous phase. In Chaos Crags, the development of reaction rims around biotite crystals is probably related to both temperature rise and water pressure decrease. The temperature of the system would rise as a result of underplating of the rhyodacite magma chamber by hot basaltic magma. If the thermal stability limit of biotite is exceeded, devolatilization in the biotites would occur. Bardintze &

Table 4: Representative analyses of plagioclase feldspars

	Clear plagioclase phenocryst		Resorbed plagioclase phenocryst in host			Resorbed plagioclase phenocryst in inclusion			Inclusion microlite		Host microlite	
	core	rim	core	inside rim	outside rim	core	inside rim	outside rim	core	rim	core	rim
SiO_2	60·85	59·31	58·57	48·75	57·73	60·89	50·41	51·32	52·18	57·13	48·80	52·41
Al_2O_3	24·13	25·36	25·73	32·13	26·60	23·74	30·84	29·90	29·47	26·75	32·01	29·34
FeO	0·22	0·25	0·26	0·67	0·38	0·25	0·54	0·51	0·73	0·37	0·61	0·50
CaO	6·14	7·36	7·44	15·42	8·53	5·61	14·00	13·24	12·84	9·02	15·23	12·40
K_2O	0·62	0·48	0·47	0·08	0·40	0·69	0·11	0·14	0·09	0·37	0·06	0·14
Na_2O	7·91	7·24	7·19	2·82	6·38	8·03	3·52	3·89	4·31	6·41	2·76	4·61
Total	99·88	99·99	99·67	99·86	100·01	99·22	99·42	98·99	99·62	100·04	99·47	99·41
An	29·0	35·0	35·4	74·8	41·5	26·8	68·3	64·8	61·9	42·8	75·1	59·3
Ab	67·5	62·3	61·9	24·7	56·2	69·3	31·1	34·5	37·6	55·1	24·6	39·9
Or	3·5	2·7	2·7	0·5	2·3	4·0	0·7	0·8	0·5	2·1	0·3	0·8

Bonin (1987) and Feeley & Sharp (1996) pointed out that volatile release during biotite and amphibole dehydrogenation may lead to vesiculation and eruption. When combined with volatiles released by exsolution from quenched inclusions into a water-saturated rhyodacite, there is a strong likelihood that mafic recharge is closely coupled in time with magma ascent, eruption or emplacement, causing more devolatilization in the biotites. The same eruption dynamics that produce variably thick opacite rims on amphiboles would produce similar variably thick opacite rims on biotites.

Plagioclase

Plagioclase is the most abundant mineral in the Chaos Crags domes, with large plagioclase phenocrysts and small plagioclase microlites occurring in both the inclusions and host rhyodacite. Representative analyses of all feldspar types are presented in Table 4. The large phenocrysts occur as unresorbed and partially resorbed crystals that appear to have originally crystallized largely in the host rhyodacite (see below). They are generally 5–10 mm long and euhedral to subhedral. Unresorbed plagioclase crystals in the host rhyodacite are clear euhedral crystals, weakly zoned across most of the crystal (~$An_{30–35}$) but slightly zoned near the rim (~$An_{35–40}$) (Fig. 8a). Some of the clear crystals have rounded corners, which are interpreted as caused by simple dissolution and were probably the result of raised temperature.

All plagioclase phenocrysts in the hybrid basaltic andesite inclusions have experienced various degrees of resorption (Fig. 8b). Many of these partially resorbed phenocrysts have ragged, sieve-textured cores that extend out to the rim, which may be a function of the thin section level; however, most are not fully resorbed and have sieve-textured resorption surfaces only a few tens of microns thick surrounding a clear core. The clear cores are compositionally identical to the host rhyodacite plagioclase phenocrysts (~$An_{30–35}$). All partially resorbed plagioclase crystals in the inclusions have a clear overgrowth rim that is a few tens of microns thick and strongly normally zoned; this rim tends to restore the euhedral outline of the crystal, probably reflecting reattainment of equilibrium between the plagioclase crystals and the basaltic andesite magma. Compositionally, the rims are approximately An_{75} on the inside of the rim and An_{50} near the crystal edge.

Resorbed plagioclase phenocrysts also occur in the host rhyodacite (Fig. 8c). They are ~5–10 mm long, have variably resorbed cores which extend out to the rim, and are surrounded by clear, strongly normally zoned overgrowth rims. The composition of the crystals is approximately $An_{30–35}$ in the core, increases in An content throughout the sieve-textured zone, and becomes approximately An_{75} near the inside edge and An_{50} near the crystal edge of the overgrowth rims. These are equivalent to the partially resorbed plagioclase phenocrysts in the inclusions that have been released from the inclusions back into the host rhyodacite.

Resorbed plagioclase phenocrysts in both inclusions and rhyodacite have sieve textures to a variable extent. The sieve zones consist of micrometer-scale channels of glass and plagioclase, irregularly truncating primary interior planar growth zones. The texture is the result of immersion of sodic plagioclase phenocrysts into a hotter melt and in equilibrium with more calcic plagioclase phenocrysts. This texture has been reproduced in

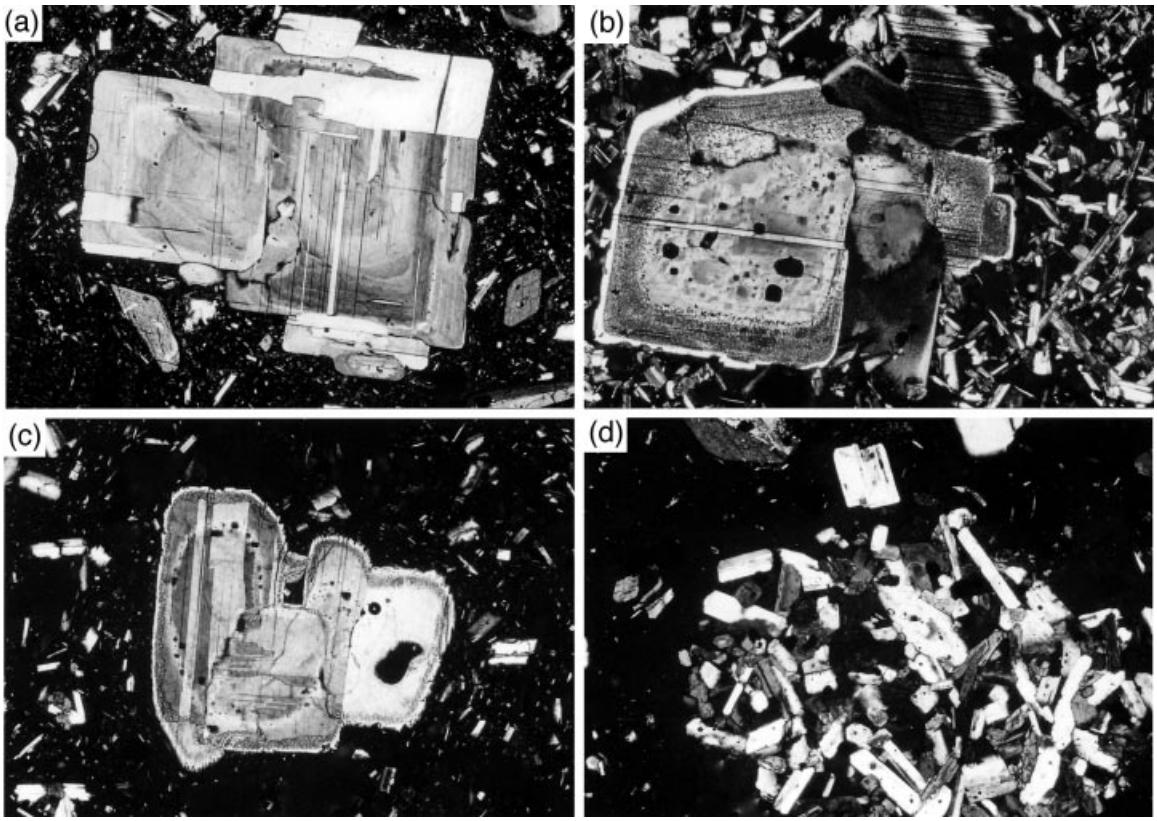

Fig. 8. Textural relations of plagioclase in Chaos Crags lavas. (a) Clear, unresorbed plagioclase phenocryst in host dacite. Field of view is ~4 mm. (b) Plagioclase phenocryst with sieve-textured, resorption-generated zone in hybrid magmatic inclusion. The development of a sieve zone surrounding a relatively clear core, and development of clear, euhedral, normally zoned rim surrounding the whole crystal should be noted. Field of view is ~2 mm. (c) Resorbed plagioclase phenocryst in host rhyodacite, almost identical to resorbed plagioclase crystals in hybrid basaltic andesite inclusions. The crystal has a similar sieve-textured, resorption-generated zone, and the clear plagioclase rim survived the transition from inclusion back into the host. Field of view is ~4 mm. (d) Microlites in inclusion; in this case, a mafic fragment from a disaggregating inclusion. Microlites also occur as single crystals floating in a rhyodacitic groundmass having the same composition as microlites from the magmatic inclusions. Field of view is ~2 mm.

experiments by Tsuchiyama (1985), supporting our hypothesis that the large plagioclase crystals are originally from the host rhyodacite, some of which was incorporated into a hotter, more calcic magma.

Acicular plagioclase microphenocrysts up to ~0·5 mm in length are the major component in inclusions but also occur in the host rhyodacite (Fig. 8d). The cores of the microphenocrysts are ~An_{75} and have strong normal zoning to ~An_{50} at their rims in both inclusions and rhyodacite. The zoning pattern in the microphenocrysts duplicates the zoning pattern in the overgrowth rims of the partially resorbed plagioclase phenocrysts in the inclusions; this feature suggests that they crystallized in a common undercooling environment. The microphenocrysts in the rhyodacite, therefore, are interpreted as originating from the hybrid basaltic andesite inclusions that have been disaggregated, and mingled into the host rhyodacite. Clynne (1999) has documented similar textures that demonstrate this disaggregation process.

Figure 9 shows the similarity of compositions between the clear zones in unresorbed and partially resorbed plagioclase phenocrysts from the rhyodacite and the inclusions. The increase in An content in the sieve-textured zones probably reflects fine Ca-rich plagioclase-melt material (Tsuchiyama, 1985). Also, the clear rims surrounding the partially resorbed plagioclase phenocrysts in both inclusions and the host rhyodacite have similar strong normal zoning.

Bulk-rock chemistry

Bulk-rock geochemical data for both the inclusions and host rhyodacite are consistent with simple binary mixing between two end-member magmas, basalt and rhyodacite. On oxide–oxide diagrams this is reflected by extremely good linear correlations, considering the 15–20% SiO_2 di erence; the distinction between the lithologic groups defined above for the rhyodacites is apparent

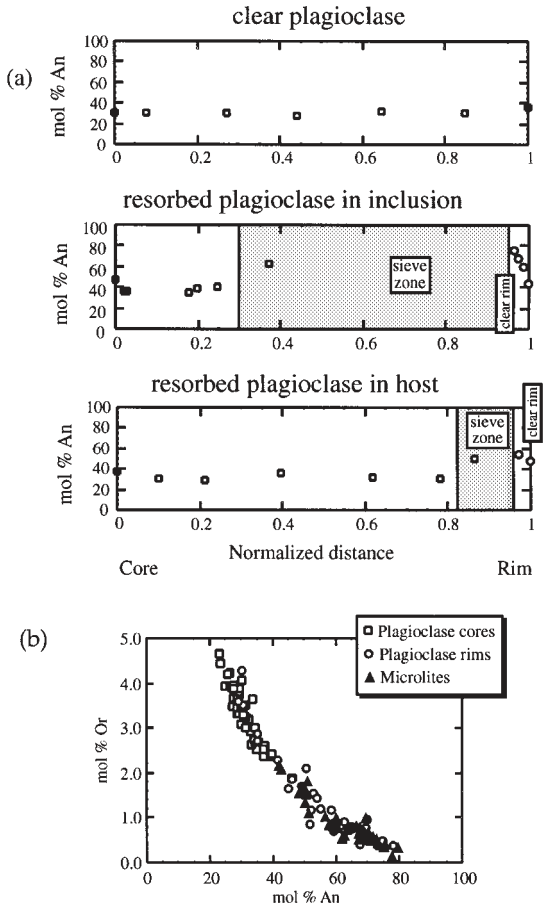

Fig. 9. Compositional relationships between di erent plagioclase crystals in Chaos Crags lavas. (a) Representative traverses of clear phenocrysts in the host and partially resorbed plagioclase phenocrysts in both host and inclusions showing compositional data and their relationship to cores of crystals, sieve zones, and clear rims. (b) Compositions of plagioclase phenocrysts and microlites plotted as mol % An vs mol % Or in the ternary system An–Ab–Or. It should be noted that clear normally zoned rims on partially resorbed plagioclase phenocrysts span the same compositional range as the normally zoned inclusion and host microlites.

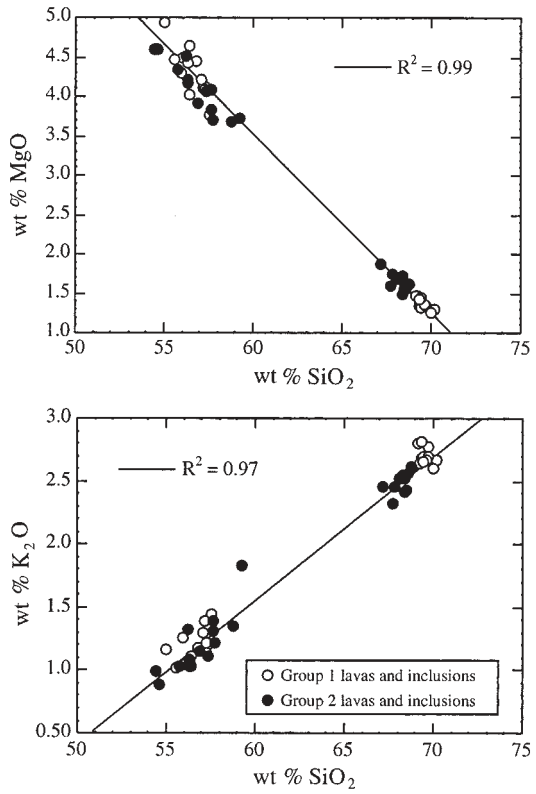

Fig. 10. Plots of MgO and K_2O vs SiO_2 for Group 1 and Group 2 inclusions and host rocks. The excellent fit of the data over 15–20 wt % in SiO_2 confirms mixing origin of Chaos Crags inclusions and host. It should be noted that an excellent fit occurs for all other oxide components.

(Fig. 10). The earlier, Group 1 domes (A and B) and the later, Group 2 domes (C, D, E and F) form tight cohesive groups with little scatter about or along the mixing line. The inclusion compositions are more scattered along the line but are collinear with the dome rhyodacite, together defining mixing lines. There is no distinction in composition in the inclusions between the earlier and later domes. The scatter of inclusions along the line represents the incorporation of more rhyodacitic material into the inclusions during the inclusion-forming process. Scatter of inclusions about the line is probably due to analytical uncertainty or to some type of fractionation of one or more of the oxide components. In this case, it is probably gain or loss of residual liquid in the inclusions (e.g. see Bacon, 1986).

Isotope systematics of whole rocks

Strontium isotopic data were collected on whole-rock samples to determine the extent of isotopic di erences between host dome rocks and inclusions (Table 5 and Fig. 11). As stated previously, this study focuses on the initial domes, for which we postulate that the isotopic di erences are greatest, and the final dome, where the isotopic di erences are least. Even though data from rocks of domes C, D, and E are sparse, the isotope data overall show that, in most cases, the host rock ratios have a slight spread in values, which generally decrease with sequential dome emplacement. The inclusions also cover a range in $^{87}Sr/^{86}Sr$ ratios with the most primitive bulk compositions characterized by distinctly lower $^{87}Sr/^{86}Sr$ ratios, except for dome D in which the inclusion $^{87}Sr/^{86}Sr$ ratios are higher than many of the host-rock $^{87}Sr/^{86}Sr$ ratios. These data suggest either that there is involvement of a di erent mafic magma, or that the basalt or hybrid basaltic andesite inclusions are contaminated

Table 5: Whole-rock isotope values for pyroclastic flows, host and inclusions of domes A–F (see Fig. 1*)*

Sample	Dome	$^{87}Sr/^{86}Sr$ host	$^{87}Sr/^{86}Sr$ inclusion
LC84-420	Pfa	0·704011±10	—
LC84-421	Pfb	0·704012±10	—
3	A	0·704061±10	0·703738±11
17	A	0·704025±10	0·703696±10
18	A	0·704010±10	0·703721±11
19	A	0·704026±11	—
26	A	0·704014±11	0·703664±11
27	A	—	0·703696±10
28	A	0·704038±11	0·703776±11
LC84-422	Pfc	0·704028±10	—
4	B	0·704070±11	0·703797±13
5(a)	B	0·704074±11	0·703759±10
5(b)	B	0·704056±11	0·703751±10
6	B	0·704056±09	0·703751±09
7	B	0·704013±10	0·703727±11
21	B	0·704039±09	—
29	B	—	0·703743±13
30	B	—	0·703716±11
33	B	0·704029±10	0·703676±10
34	B	—	0·703676±11
LC85-717	B	—	0·703650±09
12	C	0·704028±11	0·703779±11
15	C	0·703995±10	—
20	C	0·703945±10	0·703777±13
35	C	0·703998±10	—
8	D	—	0·703989±09
9	D	0·703972±09	0·704159±10
11	E	0·703976±10	0·703708±10
22	E	—	0·703701±10
23	E	0·703980±10	0·703734±10
24	E	—	0·703735±10
13	F	0·704008±10	0·703798±11
14	F	0·703988±09	0·703891±10
25	F	—	0·703696±10
31	F	0·703972±10	0·703764±14
32	F	0·703934±13	0·703658±11
CC4(a)	F	0·704027±11	0·703766±11
CC4(b)	F	0·704058±14	0·704076±14
CC5	F	0·703979±11	0·704084±13

Pfa and Pfb, and Pfc are pyroclastic flows related to the emplacement of dome A and dome B, respectively.

by a source with higher $^{87}Sr/^{86}Sr$ ratios. Bullen & Clynne (1990) have shown that rocks of basaltic andesite and andesite composition in the Lassen Volcanic Center

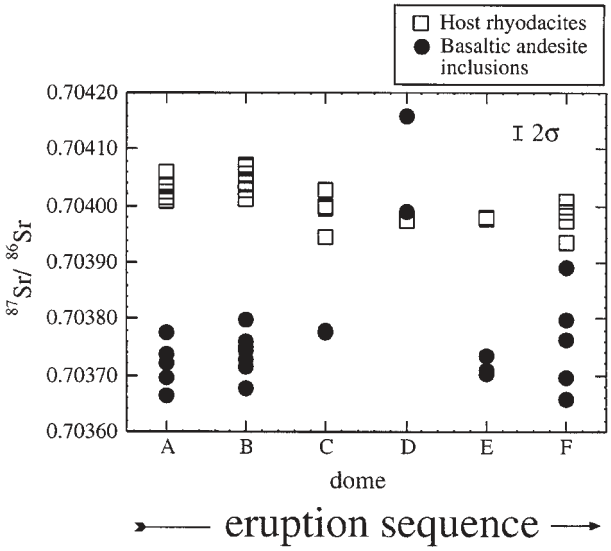

Fig. 11. Whole-rock $^{87}Sr/^{86}Sr$ ratios for host rhyodacites and respective inclusions for all domes. Symbols are approximate size of analytical uncertainty.

have diverse $^{87}Sr/^{86}Sr$ isotopic compositions ranging from 0·7029 to 0·7042. They concluded that this isotopic variability primarily reflects that of mantle-derived regional mafic magmatism with minimal interaction with middle- to upper-crustal rocks during ascent. The isotopic variability of inclusions in dome D, therefore, probably reflects involvement of a slightly di erent mafic magma. In general, however, the conclusion reached from these data is that isotopic di erences become smaller with time, reflecting greater mixing between the respective component reservoirs.

Isotope systematics of mineral phases

Petrographic and geochemical data require that at least two di erent magmas and their constituent mineral phases have been exchanged in the production of the Chaos Crags lavas. The two rock types, the hybrid basaltic andesite inclusions and the host rhyodacite, are isotopically distinct (Fig. 11). If vestiges of these components retain their physical identity (early formed crystals from magmas that have subsequently hybridized), then they may also retain their original isotopic compositions. A simple method of testing this suggestion is by use of strontium-isotopic analyses of the cores and rims of the exchanging crystals [i.e. 'crystal isotope stratigraphy', described by Davidson & Tepley (1997) and Davidson *et al.* (1998)].

We have determined crystal isotope stratigraphy on several plagioclase crystals from the Chaos Crags lavas. We have focused on the early eruptive domes (domes A

Table 6: Isotope traverses of plagioclase crystals from Chaos Crags inclusions and lavas

Sample	Dome	Resorbed plagioclase crystals in basaltic andesite inclusions and rock matrix						
			core		to		rim	rock matrix
LT93-17B	A	0·704035±39	0·704039±11	—	—	0·703959±15	0·703743±26	
LT93-17C	A	0·7404027±16	0·704059±13	0·704026±14	0·705013±71	0·703768±13	0·703778±11	0·703713±14
LT94-27A	A	—	0·704032±10	—	0·704014±11	0·703951±11		
LT93-06	B	—	0·704045±13	—	0·704040±13	—	0·703802±11	
LT94-30	B	0·703989±14	0·704170±14	0·704026±13	0·703932±13	0·703862±21	0·703708±13	0·703685±14
LT93-13A	F	0·703874±25	0·703927±11	—	0·703854±11	—	0·703780±16	
LT93-13B	F	—	0·704011±16	—	0·704002±14	0·703910±13	0·703781±16	
		Plagioclase crystals in rhyodacite host						
LT93-17A	A	—	0·704051±13	0·704019±11	—	—		
LT93-13C	F	—	0·704012±13	0·704043±13	—	0·703933±11		

and B) because, as the whole-rock isotopic data indicate, the isotopic di erences between the end members are the greatest; however, crystals from a later dome (dome F) have also been drilled to monitor the homogenization process. We have focused on two groups of plagioclase phenocrysts: the large, partially resorbed plagioclase crystals in the hybrid basaltic andesite inclusions, and the large, partially resorbed plagioclase crystals that now reside in the host rhyodacite. As noted above, petrographic and major-element data suggest that these groups of crystals are in fact the same, with one group having found its way back into the host rhyodacite. Drill hole $^{87}Sr/^{86}Sr$ ratios of nine crystals from three di erent domes, most of which are from the hybrid basaltic andesite inclusions, are listed in Table 6.

Isotope traverses were conducted on several partially resorbed plagioclase phenocrysts enclosed within hybrid basaltic andesite inclusions. These crystals are typically large and, in terms of An content $\sim An_{30–35}$, compositionally similar to those in the host rhyodacite. Many crystals have sieve textures indicating that the crystals were immersed in an environment hotter and more calcic than the environment of the equilibrium plagioclase. Nomarski imaging shows that the growth histories of the crystals are defined by many fine oscillatory zones punctuated by multiple, major dissolution surfaces with irregular boundaries and calcic zones (Type II zoning); this feature also supports this hypothesis. All crystals studied have a distinct overall drop in the $^{87}Sr/^{86}Sr$ ratio from core to rim. Below, we discuss the integration of Sr-isotope data with compositional and petrographic data for plagioclase phenocrysts from three hybrid basaltic andesite inclusions and another from a dome rhyodacite.

LT94-27A is resorbed plagioclase from a hybrid basaltic andesite inclusion of dome A (Fig. 12). The plagioclase crystal is ~3·5 mm in radius, has several dissolution zones truncating substratal, finer-scale oscillatory zones, and has a distinct ~0·3 mm wide sieve zone. An electron microprobe traverse of this crystal indicates relatively constant composition of An_{35} punctuated by large variations in An content (Type II zoning). Near the edge of the crystal, the An content increases through the sieve zone to An_{53} at the edge of the crystal. The clear rim was not analyzed for An content but can be estimated from the composition of plagioclase microlites in the inclusions to be $\sim An_{60–75}$ (Table 4). Oscillatory zoning is represented by shifts in the An content of ~3–5 mol % (Type I zoning). Abrupt shifts in An content of up to 15 mol % locally along the traverse correspond to major dissolution surfaces easily discernible on the NDIC image and indicated by the arrows across Fig. 12.

Three Sr microanalysis holes were drilled in this crystal (see Fig. 12). The core $^{87}Sr/^{86}Sr$ ratio is similar to that of the host rhyodacite (see Table 6), whereas the sieve zone and the clear overgrowth-rim $^{87}Sr/^{86}Sr$ ratios are slightly lower. The isotopic composition of the rim is not quite as low as that of the inclusions, probably because the scale of sampling is larger than the width of the rim itself, resulting in mechanical mixing of rim Sr with Sr from the interior the crystal.

LT94-30 (Fig. 13) is a plagioclase crystal from a hybrid basaltic andesite inclusion of dome B. Part of Group 1, this sample represents a crystal from an early eruptive dome that should behave similarly to samples from dome A. This crystal is ~1 cm long, shows numerous truncations

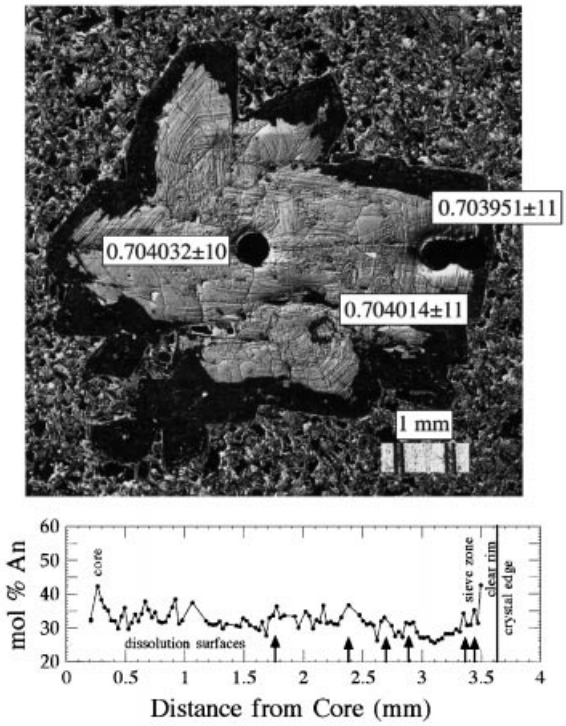

Fig. 12. Nomarski image, electron microprobe traverse, and $^{87}Sr/^{86}Sr$ ratios from drill holes of a partially resorbed plagioclase crystal (LT94-27A) from dome B. The image shows distinct growth and dissolution zones, a sieve area resulting from partial resorption, and a clear rim surrounding the crystal and in contact with hybrid basaltic andesite groundmass. The electron probe traverse corresponds to a line from the middle drill hole extending right to the two drill holes near the edge of the crystal. Distinct changes in An content correspond to growth and dissolution zones on the crystal. (See text for details.)

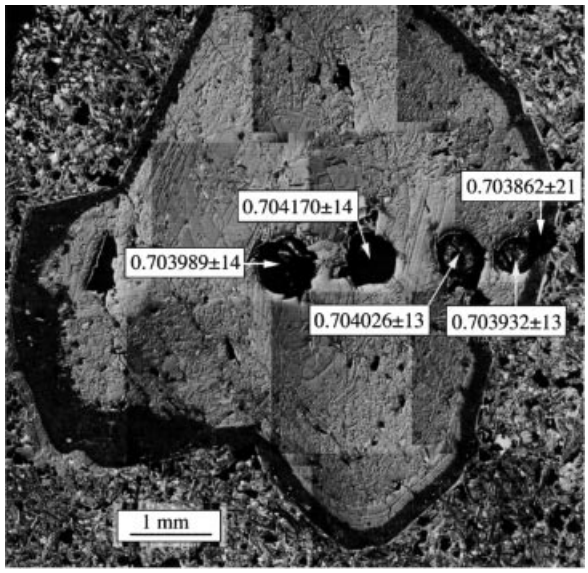

Fig. 13. Nomarski image and $^{87}Sr/^{86}Sr$ ratios from drill holes in a partially resorbed plagioclase crystal (LT94-30) from dome A. The crystal distinctly shows a relatively clear core, a partially resorbed or sieve-textured zone around the crystal, and a thin, clear rim surrounding the whole crystal. Large, black holes are sample site drill holes, which sample both inside the crystal and out into surrounding inclusion matrix.

and dissolution surfaces within the crystal, and is surrounded by a sieve zone of ~200–750 μm thickness, and a clear rim of 5–10 μm thickness. Several holes were drilled from the core of the crystal through the rim and into the surrounding matrix. Table 6 shows that the $^{87}Sr/^{86}Sr$ ratio of the core is similar to that of the host rhyodacite but dramatically decreases through the rim matrix sites to the $^{87}Sr/^{86}Sr$ ratio of the hybrid basaltic andesite inclusion whole-rock value.

Data from LT94-27A and LT94-30 suggest that these crystals initially grew in the host rhyodacite, acquired their $^{87}Sr/^{86}Sr$ ratios, were then enveloped by the lower-$^{87}Sr/^{86}Sr$ hybrid basaltic andesite inclusion, and grew rims in equilibrium with this lower-$^{87}Sr/^{86}Sr$ magma. LT93-17A, a large, partially resorbed plagioclase crystal in the host rhyodacite from dome A, has the same textural features and the same decrease in $^{87}Sr/^{86}Sr$ ratio from core toward the rim as crystals that are now in the hybrid basaltic andesite inclusions. Figure 14 plots the $^{87}Sr/^{86}Sr$ ratio of drill holes along crystal traverses versus the normalized distance of partially resorbed plagioclase crystals sampled in this study. In all cases, the $^{87}Sr/^{86}Sr$ ratio decreases toward the rim of the crystal.

To ascertain the e ects of mixing later in the sequence of dome extrusion, we examined LT93-13A and LT93-13B, plagioclase crystals from inclusions in dome F, for strontium microanalysis. These crystals were not imaged using NDIC nor analyzed for major-element composition; however, both crystals have the same characteristic general decrease in $^{87}Sr/^{86}Sr$ ratios form cores to rims (see Table 6 and Fig. 14). The $^{87}Sr/^{86}Sr$ ratio of the core of sample LT93-13A is slightly lower than that of most cores of crystals analyzed, probably because we drilled o center to the low side. The data show the $^{87}Sr/^{86}Sr$ ratios increasing then decreasing to the hybrid basaltic andesite inclusion values near the rim. Data for LT93-13B show the characteristic decrease to the rim. A partially resorbed plagioclase phenocryst (LT93-13C) in the host rhyodacite of dome F, the last dome to erupt, was examined for the same purpose. The data show the same decrease in $^{87}Sr/^{86}Sr$ ratio from the core to the rim, suggesting that the process of plagioclase resorption and multiple recycling was still operating later in the eruption sequence.

An alternative explanation for the uniformly decreasing $^{87}Sr/^{86}Sr$ ratios in the plagioclase crystals is self-di usion, which could produce partial equilibration of a uniformly homogeneous plagioclase crystal immersed in a hot, mafic

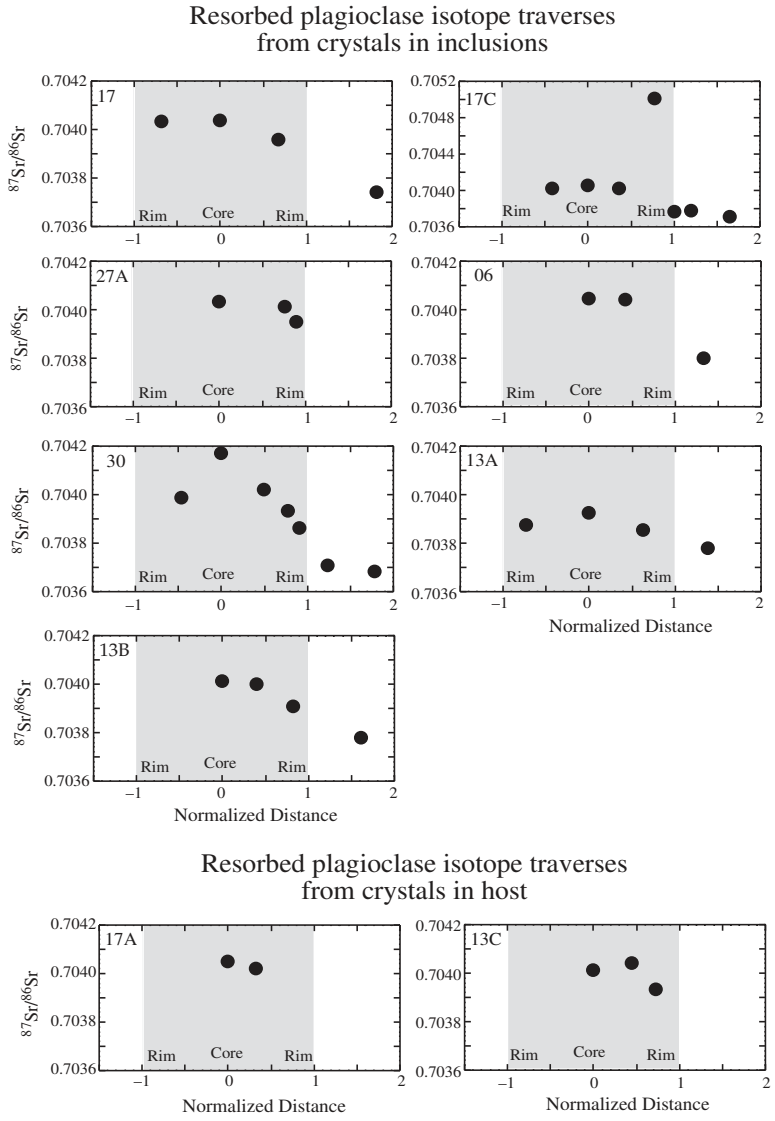

Fig. 14. $^{87}Sr/^{86}Sr$ ratios plotted against normalized distances for partially resorbed plagioclase phenocrysts from inclusion and host crystals examined in this study. The large black dots represent sample site drill holes from which strontium isotopic data were collected. The black dots do not represent drill hole size or analytical uncertainty of isotopic analysis. Distances between the center hole and the crystal edge were used as normalizing distances from which to compare locations of other drill holes within the crystal, outside but alongside the crystal, and between other di erent-sized crystals. Shaded areas are representative of crystal extents. It should be noted that sample 17C has a di erent $^{87}Sr/^{86}Sr$ scale from the rest of the samples.

magma with a lower $^{87}Sr/^{86}Sr$ ratio. However, simple modeling of $^{87}Sr/^{86}Sr$ profiles using di usion coe cients of Giletti & Casserly (1994) and equations of Christensen & DePaolo (1993) yields unrealistically long residence times (~10^5–10^6 years) of plagioclase crystals in hybrid basaltic andesite inclusions. The inferred size of the Chaos Crags magma chamber is small based on the small erupted volume of material (~2 km^3). In 10^5–10^6 years, a small, isolated molten body of magma at a shallow level in the crust would probably solidify, on the basis of parameters o ered by Spera (1980).

DISCUSSION AND PETROGENETIC MODEL

The petrographic, chemical, and isotopic evidence suggests that Chaos Crags resulted from the complex interaction of a mafic magma and a felsic magma. Plagioclase, biotite, hornblende and quartz crystals, originally crystallized in the rhyodacite, occur as partially resorbed crystals in the hybrid basaltic andesite inclusions. Olivine crystals in the host rhyodacite, occurring alongside quartz crystals, have the same composition as those in the hybrid

basaltic andesite inclusions. Inclusion debris, including inclusion microlites and partially resorbed plagioclase crystals, are scattered throughout the rhyodacite host. This evidence indicates that variably quenched hybrid basaltic andesite inclusions disaggregated, mixing their contents (including resorbed and rimmed plagioclase phenocrysts and di erentiated liquid) back into the host rhyodacite (e.g. Clynne, 1989, 1999).

In this system, the pathways of crystals are well constrained and supported by the observations described above. These observations imply that crystal populations derived from distinct magmas have exchanged as the magmas interact. A mechanism for the interaction of these magmas is therefore required. The model proposed is necessarily not as rigorously constrained as the crystal pathway interpretations but is based on experimental or theoretical considerations presented elsewhere in the literature. We stress that this is just one interpretation using well-constrained observations, and that other interpretations, using the same observations, could be equally plausible.

Magma–magma mixing of mafic and silicic components on a magma-chamber scale cannot explain all of the chemical and mineralogical features of the Chaos Crags dome-inclusion system. Complete and intimate mixing can only occur when the mass fraction of the mafic end member is large ($\geq$50%) or where the compositional di erences between magmas are small ($\leq$10 wt % SiO_2) (Kouchi & Sunagawa, 1985; Bacon, 1986; Sparks & Marshall, 1986; Nixon & Pearce, 1987; Nixon, 1988). Such large-scale mixing would produce large proportions of homogeneous intermediate-composition lavas, which are common in rocks of the Lassen Volcanic Center (Clynne, 1999) but are not present at Chaos Crags. Below ~50% of the mafic component, the result of interaction between the dominantly silicic component and the mafic component is the formation of undercooled magmatic inclusions.

The inclusion-forming process is, however, only partly responsible for the chemical and isotopic diversity observed between rocks and phases therein. Before inclusion formation, there must have been some interaction between the original magmas, involving complete magma mixing (Fig. 15). Our model suggests that the rhyodacitic magma in a chamber beneath Chaos Crags originally crystallized phenocrysts of plagioclase, quartz, biotite, and hornblende. The $^{87}Sr/^{86}Sr$ ratios of dome whole-rock samples and of cores drilled from unresorbed plagioclase crystals within those rocks indicate they originally crystallized together. An injection of hotter, less viscous basalt ponded at the base of this crystal-rich, rhyodacitic magma chamber (e.g. Wiebe, 1993, 1996) (Fig. 15a). A small proportion of rhyodacitic magma and its phases must have been homogeneously mixed with the basaltic magma, incorporating crystals of plagioclase, biotite, hornblende, and quartz that originally were in chemical and isotopic equilibrium with the rhyodacitic melt. Cores of partially resorbed plagioclase crystals in the inclusions have identical $^{87}Sr/^{86}Sr$ ratios to unresorbed plagioclase crystals in the host dome rocks. This could have produced a hybrid mafic magma, a basaltic andesitic magma, which subsequently would have interacted with the rhyodacitic magma to form the inclusions (Fig. 15).

Experiments have demonstrated that intruding magma may entrain a resident magma owing to the turbulence of the injection, producing a hybrid magma along the interface (e.g. Campbell & Turner, 1986, 1989). Entrainment of small volumes of rhyodacite into basalt along the mafic–silicic interface through viscous drag may form the hybrid basaltic andesite magma (Campbell & Turner, 1986, 1989). This allows mixing of thermally and compositionally diverse magmas because the mafic-to-silicic ratio along the interface is high for a short time, in accord with thermal and fluid-dynamical constraints (e.g. Sparks & Marshall, 1986). Alternatively (and probably related), Kouchi & Sunagawa (1985) produced a hybrid magma by forced convective mixing of basaltic and dacitic magma. Dacitic drops were torn from the interface and trapped in a large volume of basaltic liquid, readily producing a homogenized andesitic composition. Furthermore, the addition of phenocrysts considerably increased the e ciency of mixing because of smaller-scale mechanical mixing. In either case, laboratory experiments have shown that if certain criteria are met, magmas with large contrasts in viscosity and composition may partially mix.

A hybrid layer is produced by viscous shearing along the interface of rhyodacite and intruding basalt (Fig. 15b). Small volumes of rhyodacitic magma are mixed into the upper surface of the intruding basaltic magma, maintaining a large proportion of basalt to rhyodacite. Variability in the compositional and isotopic data of the hybrid basaltic andesite inclusions illustrates the small but varied amount of rhyodacite and basalt that mixed together (see Figs 10 and 11). Also mixed into the basalt are phenocryst phases from the rhyodacite, which have compositional and isotopic values di erent from the basalt. This forms a hybrid layer, which is a combination of basaltic liquid with phases with low $^{87}Sr/^{86}Sr$ ratios and rhyodacitic liquid with phases with higher $^{87}Sr/^{86}Sr$ ratios.

The thermal profile of the hybrid layer contributes to the production of inclusions. A thermal gradient must exist across the hybrid layer; unmixed basalt beneath the hybrid layer is hotter than unmixed rhyodacite material above the hybrid layer, and small volumes of cooler rhyodacite are incorporated into the basalt. A small-scale convection system may develop within the hybrid layer owing to the temperature contrast across it, which would

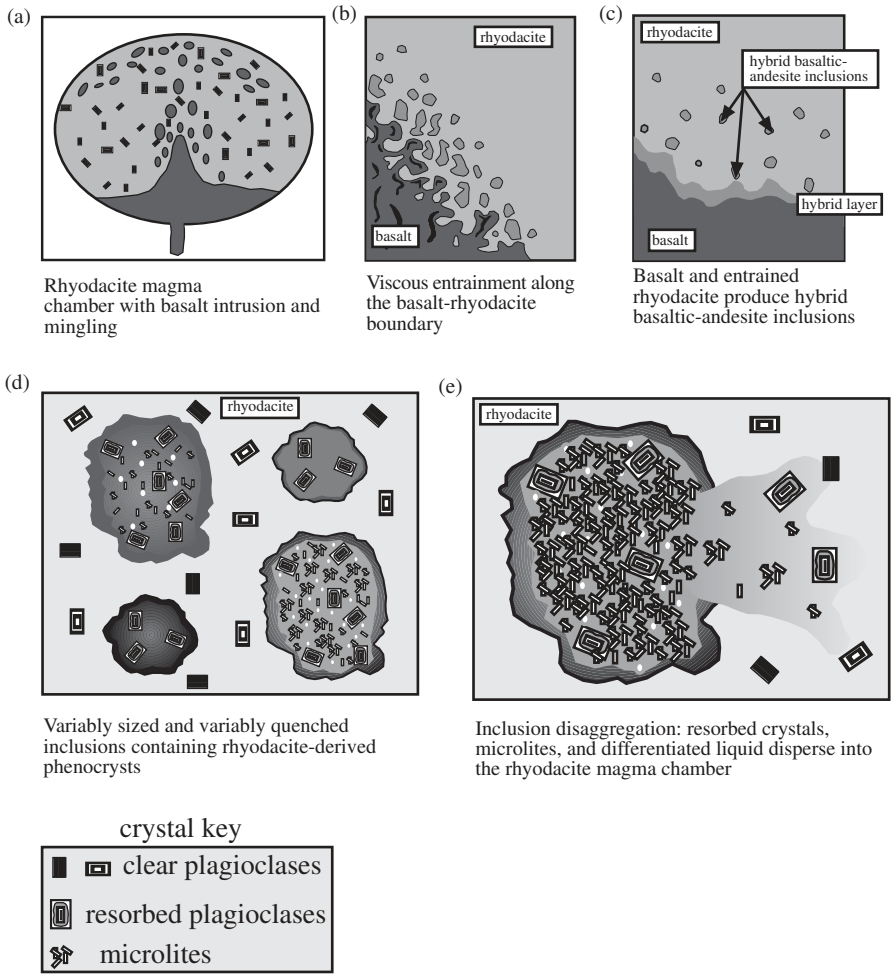

Fig. 15. Model illustrating basaltic influx into magma chamber (a), viscously entraining rhyodacitic magma along the turbulent interface (b), formation of a hybrid layer and hybrid basaltic andesite inclusions of various sizes and various degrees of quenching (c and d), and inclusion disaggregation into magma chamber dispersing partially resorbed crystals, microlites, and di erentiated liquid (e). It should be noted that the chamber configuration is entirely schematic and may bear no relation to the actual shape.

assist in homogenizing the hybrid (e.g. Kouchi & Sunagawa, 1985). As heat is transferred across the hybrid–rhyodacite interface and some cooling occurs, crystallization of the basaltic andesite hybrid proceeds, causing vapor-phase saturation. The vapor-phase exsolution causes the bulk density of the hybrid basaltic andesite magma to equal the bulk density of the overlying rhyodacite magma, creating an unstable, water-saturated layer (Eichelberger, 1980; Huppert *et al.*, 1982). Huppert *et al.* (1982) calculated that an unstable, vesiculating hybrid layer could be produced, which may thicken to a few meters and which may account for the occurrence of mafic inclusions in silicic volcanic rocks.

Rhyodacite-derived plagioclase crystals incorporated into the basalt react to the thermal and chemical disequilibrium. Immersion of crystals into a hotter, more calcic melt causes the crystals' edges to disintegrate into a fine crystal–melt mixture, producing partially resorbed or sieve-textured plagioclase crystals (Tsuchiyama, 1985). The composition of the sieve zone becomes more calcic and is thought to be controlled largely by di usion in the melt and partially by di usion in the crystal (Tsuchiyama, 1985). Similar thermal and chemical disequilibrium reactions take place with other rhyodacite-derived phenocrysts mixed into the basalt. Biotite and hornblende recrystallize into pyroxene, plagioclase and oxides, and quartz is resorbed around which pyroxene coronae form.

Instability in the hybrid layer caused by convective currents, density variability between the basaltic andesite and the rhyodacite, or periodic infusions of fresh mafic magmas may lead to release of blobs of hybrid magma into the overlying rhyodacitic magma (Fig. 15c). Because many of the hybrid inclusions have quenched margins,

thermal equilibration between the rhyodacite magma and hybrid inclusions occurs after the blobs are separated from the hybrid layer. As the blobs move into the cooler rhyodacite magma, many inclusions are quenched; this traps volatile phases within the inclusions to produce low-density, self-contained blobs of hybrid basaltic andesite magma. The chilled margin may act as a barrier to gas bubbles, allowing the inclusions to behave as suspended low-density, partially solid, lumps (Bacon, 1986). Additionally, as the inclusions are quenched in the rhyodacite magma, crystallization occurs rapidly. Clear, strongly normally zoned rims form around the resorbed feldspars, and microlites of similar compositional zoning crystallize. The rims around the feldspars also acquire the isotopic value of the bulk of the basaltic andesite inclusion (Fig. 15d).

The blobs, having a smaller e ective density than the overlying rhyodacite magma, rise or are caught in the convecting rhyodacite and disperse throughout the chamber. This allows for their distribution within the domes despite the viscosity contrast (e.g. Eichelberger, 1980; Huppert *et al.*, 1982). Shearing of the undercooled magmatic inclusions in the convecting rhyodacitic magma chamber is probably the primary mechanism for disaggregation (Fig. 15e).

Episodic infusions of hot, mafic magma, prolonged residence of hot, mafic magma beneath the rhyodacitic magma chamber, or a combination of these processes will lead to lower temperature, density and viscosity contrasts between the rhyodacite magma and the hybrid basaltic andesite layer, from which the hybrid basaltic andesite inclusions are derived. Forceful injection of hot, mafic magma into the previously heated rhyodacitic magma might allow basaltic magma to stir into the magma chamber more vigorously and turbulently than before. The result could be the production of larger and more variably quenched hybrid basaltic andesite inclusions (Fig. 15d).

The above-described processes may explain the di erences between Group 1 and Group 2 lavas. Group 1 lavas have fewer, more completely quenched inclusions, whereas Group 2 lavas have more abundant, variably quenched inclusions. Small inclusions in the early domes (Group 1) rapidly crystallized. Being smaller and more crystalline, Group 1 inclusions would be more resistant to shearing and contributed a smaller amount of disaggregated inclusion material (liquid and crystals) back into the host. Larger inclusions in the later domes (Group 2) cooled more slowly, thus allowing the enveloped plagioclase crystals to chemically and thermally resorb, and allowing the microlites in the inclusions and the clear rims on the plagioclase crystals in the inclusions to crystallize. The larger inclusions generally have thinner quenched rims, if any, and were less crystalline, which allowed them to be sheared apart more easily than smaller, more completely quenched Group 1 inclusions.

IMPLICATIONS AND CONCLUSIONS

Isotopic microsampling of crystal phases provides a definitive means of identifying open-system di erentiation histories. For plagioclase in particular, isotopic microsampling relative to textural features such as dissolution surfaces provides a crystal isotope stratigraphy, which reflects changes in magma composition.

For Chaos Crags, a complex pathway of magma mingling is indicated by the occurrence of variably quenched, hybrid basaltic andesite inclusions in rhyodacite host. Strontium-isotope analyses of clear and partially resorbed plagioclase crystals indicate that all originally crystallized in the silicic host. Some are now found in the hybrid basaltic andesite inclusions, where they are partially resorbed and rimmed with a clear overgrowth. Mechanical entrainment of crystals occurred during mixing. However, some of these crystals, together with concurrently formed microlites, have been identified in the silicic host. We demonstrate that this is due to disaggregation of the hybrid basaltic andesite inclusions. Progressive mingling of the mafic and silicic components at Chaos Crags is reflected in the convergence of host and inclusion whole-rock $^{87}Sr/^{86}Sr$ ratios through time. Such a process may be a common mechanism in the products of intermediate magmas, especially in orogenic magmas, but may be easily overlooked in the absence of macroscopic evidence such as the presence of inclusions. Isotopic microsampling is one way of testing for such processes.

ACKNOWLEDGEMENTS

The authors thank the reviewers R. L. Christiansen, D. Geist, M. J. Hibbard, J. Tepper, and R. Tilling for providing excellent and constructive comments. We also thank D. Siems, USGS analyst, for XRF analyses, F. Ramos and M. Yeager for invaluable help in the UCLA geochemistry laboratory, and the National Park Service for access to Lassen Volcanic National Park. Funding for this project was provided in part from National Science Foundation Grants EAR-9303791 and EAR-9526903 to J.P.D. and in part from Geological Society of America and Sigma Xi grants to F.J.T.

REFERENCES

Albee, A. L. & Ray, L. (1970). Correction factors for electron microanalysis of silicates and oxides, carbonates, phosphates, and sulfates. *Analytical Chemistry* **42,** 1408–1414.

Anderson, A. T. (1983). Oscillatory zoning of plagioclase: Nomarski interference contrast microscopy of etched polished thin sections. *American Mineralogist* **69,** 660–676.

Bacon, C. R. (1986). Magmatic inclusions in silicic and intermediate volcanic rocks. *Journal of Geophysical Research* **91,** 6091–6112.

Bacon, C. R. & Druitt, T. H. (1988). Compositional evolution of the zoned calc-alkaline magma chamber of Mount Mazama, Crater Lake, Oregon. *Contributions to Mineralogy and Petrology* **98,** 224–256.

Bardintze , J.-M. & Bonin, B. (1987). The amphibole e ect: a possible mechanism for triggering explosive eruptions. *Journal of Volcanology and Geothermal Research* **33,** 255–262.

Bence, A. E. & Albee, A. L. (1968). Empirical correction factors for the electron microanalysis of silicates and oxides. *Journal of Geology* **76,** 382–403.

Blundy, J. D. & Shimizu, N. (1991). Trace element evidence for plagioclase recycling in calc-alkaline magmas. *Earth and Planetary Science Letters* **102,** 178–197.

Bullen, T. D. & Clynne, M. A. (1990). Trace element and isotopic constraints on magmatic evolution at Lassen Volcanic Center. *Journal of Geophysical Research* **95,** 19671–19691.

Campbell, I. H. & Turner, J. S. (1986). The influence of viscosity on fountains in magma chambers. *Journal of Petrology* **27,** 1–30.

Campbell, I. H. & Turner, J. S. (1989). Fountains in magma chambers. *Journal of Petrology* **30,** 885–923.

Christensen, J. N. & DePaolo, D. N. (1993). Time scales of large volume silicic magma systems; Sr isotopic systematics of phenocrysts and glass from the Bishop Tu , Long Valley, California. *Contributions to Mineralogy and Petrology* **113,** 100–114.

Christiansen, R. L., Clynne, M. A. & Mu er, L. J. P. (1999). Geologic map of the area of Lassen Peak, Chaos Crags, and Upper Hat Creek, California. Scale 1:24 000. US Geological Survey (in press).

Clynne, M. A. (1989). Disaggregation of quenched magmatic inclusions contributes to chemical diversity in silicic lavas of Lassen Peak, California. *Bulletin of the New Mexico Bureau of Mines and Mineral Resources* **131,** 54.

Clynne, M. A. (1990). Stratigraphic, lithologic, and major element geochemical constraints on magmatic evolution at Lassen Volcanic Center, California. *Journal of Geophysical Research* **95,** 19651–19669.

Clynne, M. A. (1999). Complex magma mixing origin for multiple volcanic lithologies erupted in 1915, from Lassen Peak, California. *Journal of Petrology* **40,** 105–132.

Clynne, M. A. & Mu er, L. J. P. (1989). Lassen National Park and vicinity. In: Mu er, L. J. P. (ed.) *IAVCEI Excursion 12B, South Cascade Arc Volcanism, California and Southern Oregon. New Mexico Bureau of Mines and Mineral Resources Memoir* **47,** 183–225.

Davidson, J. P. & Tepley, F. J. III (1997). Recharge in volcanic systems: evidence from isotopic profiles of phenocrysts. *Science* **275,** 826–829.

Davidson, J. P., Tepley, F. J. III & Knesel, K. (1998). Isotopic fingerprinting may provide insights into evolution of magmatic systems. *Eos Transactions, American Geophysical Union* **79,** 185, 189, 193.

Eichelberger, J. C. (1978). Andesitic volcanism and crustal evolution. *Nature* **275,** 21–27.

Eichelberger, J. C. (1980). Vesiculation of mafic magma during replenishment of silicic magma reservoir. *Nature* **288,** 446–450.

Feeley, T. C. & Sharp, Z. D. (1996). Chemical and hydrogen isotopic evidence for *in situ* dehydrogenation of biotite in silicic magma chamber. *Geology* **24,** 1021–1024.

Giletti, B. J. & Casserly, E. D. (1994). Strontium di usion kinetics in plagioclase feldspars. *Geochimica et Cosmochimica Acta* **58,** 3785–3793.

Grove, T. H., Baker, M. B. & Kinzler, R. J. (1984). Coupled CaAl–NaSi di usion in plagioclase feldspar: experiments and applications to cooling rate speedometry. *Geochimica et Cosmochimica Acta* **48,** 2113–2121.

Gu anti, M. & Weaver, C. S. (1988). Distribution of late Cenozoic volcanic vents in the Cascade Range: volcanic arc segmentation and regional tectonic considerations. *Journal of Geophysical Research* **93,** 6513–6529.

Haase, C. S., Chadam, J., Feinn, D. & Ortoleva, P. (1980). Oscillatory zoning in plagioclase feldspar. *Science* **209,** 272–274.

Heiken, G. & Eichelberger, J. C. (1980). Eruptions at Chaos Crags, Lassen Volcanic National Park, California. *Journal of Volcanology and Geothermal Research* **7,** 443–481.

Huppert, H. E., Sparks, R. S. J. & Turner, J. S. (1982). E ects of volatiles on mixing in calc-alkaline magma systems. *Nature* **297,** 554–557.

Kouchi, A. & Sunagawa, I. (1985). A model for mixing basaltic and dacitic magmas as deduced from experimental data. *Contributions to Mineralogy and Petrology* **89,** 17–23.

Nixon, G. T. (1988). Petrology of the younger andesites and dacites at Iztaccihuatl Volcano, Mexico: I. Disequilibrium phenocryst assemblages as indicators of magma chamber processes. *Journal of Petrology* **29,** 213–264.

Nixon, G. T. & Pearce, T. H. (1987). Laser-interferometry study of oscillatory zoning in plagioclase: the record of magma mixing and phenocryst recycling in calc-alkaline magma chambers, Iztaccihuatl Volcano, Mexico. *American Mineralogist* **72,** 1144–1162.

Pearce, T. H. (1993). Recent work on oscillatory zoning in plagioclase. In: Parsons, I. (ed.) *Feldspars and their Reactions*. Dordrecht: Kluwer Academic, pp. 313–349.

Pearce, T. H. & Clark, A. H. (1989). Nomarski interference contrast observations of textural details in volcanic rocks. *Geology* **17,** 757–759.

Pearce, T. H. & Kolisnik, A. M. (1990). Observations of plagioclase zoning using interference imaging. *Earth-Science Reviews* **29,** 9–26.

Roeder, P. L. & Emslie, R. F. (1970). Olivine–liquid equilibrium. *Contributions to Mineralogy and Petrology* **29,** 275–289.

Rutherford, M. J. & Hill, P. M. (1993). Magma ascent rates from amphibole breakdown; an experimental study applied to the 1980–1986 Mount St Helens eruptions. *Journal of Geophysical Research* **98,** 19667–19685.

Simonetti, A., Shore, M. & Bell, K. (1996). Diopside phenocrysts from nephelinite lavas, Napak volcano, eastern Uganda: evidence for magma mixing. *Canadian Mineralogist* **34,** 411–421.

Singer, B. S., Dungan, M. A. & Layne, G. D. (1995). Textures and Sr, Ba, Mg, Fe, K, and Ti compositional profiles in volcanic plagioclase: clues to the dynamics of calc-alkaline magmas chambers. *American Mineralogist* **80,** 776–798.

Sparks, R. S. J. & Marshall, L. A. (1986). Thermal and mechanical constraints on mixing between mafic and silicic magmas. *Journal of Volcanology and Geothermal Research* **29,** 99–124.

Spera, F. (1980) Thermal evolution of plutons; a parameterized approach. *Science* **207,** 299–310.

Stamatelopoulou-Seymour, K., Vlassopoulos, D., Pearce, T. H. & Rice, C. (1990). The record of magma chamber processes in plagioclase phenocrysts at Thera volcano, Aegean volcanic arc, Greece. *Contributions to Mineralogy and Petrology* **104,** 73–84.

Stimac, J. A. & Pearce, T. H. (1992). Textural evidence of mafic–felsic magma interaction in dacite lavas, Clear Lake, California. *American Mineralogist* **77,** 795–809.

Tsuchiyama, A. (1985). Dissolution kinetics of plagioclase in the melt of the system diopside–albite–anorthite, and the origin of dusty plagioclase in andesites. *Contributions to Mineralogy and Petrology* **89,** 1–16.

Wiebe, R. A. (1993). Basaltic injections into floored silicic magma chambers. *Eos Transactions, American Geophysical Union* **74,** 1, 3.

Wiebe, R. A. (1996). Mafic–silicic layered intrusions: the role of basaltic injections on magmatic processes and the evolution of silicic magma chambers. *Transactions of the Royal Society of Edinburgh: Earth Sciences* **87,** 233–242.